For Submission to: ***Cytometry Part A.***

Title: **Analysis insights for three FRET pairs of chemically unlinked two-molecule FRET cytometry.**

Running Title: Chemically unlinked two-color FRET cytometry

Authors: Zhongran Ni[1], Alex Gale[1], Michael S Johnson[1] and Lisa M Sedger[1*]

Affiliation: [1]School of Life Science, Faculty of Science, University of Technology Sydney,

Corresponding author*: Lisa M Sedger[1], Faculty of Science,
University of Technology Sydney,
P.O. Box 123 Broadway, Sydney, NSW Australia.
Email: lisa.sedger@uts.edu.au

Key words: cytometry analysis, Cyan (C)-, red (R)-, and yellow (Y)- fluorescent protein (CFP, RFP, and YFP), cytometer, Förster or fluorescence resonance energy transfer (FRET), FlowJo, multi-dimensional reduction data, tumor necrosis factor receptor, tumor necrosis factor receptor-superfamily (TNFR-SF).

List of abbreviations: Fluorescent protein, FP; Förster (fluorescence) energy resonance transfer, FRET; mean fluorescence intensity, MFI; photomultiplier tube, PMT; Tumor Necrosis Factor Receptor (TNFR), Tumor Necrosis Factor Receptor-Superfamily (TNFR-SF).

ABSTRACT. (300s words)

Förster resonance energy transfer (FRET) is the direct energy exchange between two-component fluorescent molecules. FRET methods utilize chemically linked molecules or unlinked fluorescence protein-protein interactions. FRET is therefore a powerful indicator of molecular proximity, but standardized determination of FRET efficiency is challenged when investigating natural (chemically unlinked) interactions. In this paper, we have examined the interactions of tumor necrosis factor receptor-1 (TNFR1) molecules expressed as recombinant fusion proteins of cyan, yellow, or red fluorescent protein (-CFP, -YFP, or -RFP) to evaluate two-molecule chemically unlinked FRET by flow cytometry. We demonstrate three independent FRET pairs CFP→YFP (FRET-1), YFP→RFP (FRET-2) and CFP→RFP (FRET-3), comparing TNFR1+TNFR1 with non-interacting TNFR1+CD27 proteins, on both LSR-II and Fortessa X-20 cytometers. We describe genuine FRET activities reflecting TNFR1 homotypic interactions. FRET events can be visualized during sample acquisition via the use of "spiked" FRET donor cells, together with TNFR1+TNFR1 co-transfected cells, as FRET channel MFI overlays. FRET events are subsequentially indicated by comparing concatenated files of cells expressing either FRET positive events (TNFR1+TNFR1) or FRET negative events (TNFR1+CD27) to generate single-cell scatter plots showing loss of FRET donor brightness. Robust determination of FRET efficiency is then confirmed at the single-cell level by applying matrix calculations based on the measurements of FRET donor, acceptor and FRET fluorescent intensities (*I*), detector channel emission coefficient (*S*), fluorescent protein extinction coefficients (ε) and α factor. In this TNFR based system, the mean CFP→YFP FRET-1 efficiency is 0.43 (LSR-II) and 0.41 (Fortessa), the mean YFP→RFP FRET-2 efficiency is 0.30 (LSR-II) and 0.29 (Fortessa), and the mean CFP→RFP FRET-3 efficiency is 0.56 (LSR-II) and 0.54 (Fortessa). This study also embraces multidimensional clustering using t-SNE, Fit-SNE, UMAP, Tri-Map and PaCMAP to further demonstrate FRET. These approaches establish a robust system for standardized detection of chemically unlinked TNFR1 homotypic interactions with three individual FRET pairs.

INTRODUCTION.

The interactions of two proteins are often examined biochemically, but this is traditionally in non-dynamic experimental conditions such as those used in sample lysates for immunoprecipitation and Western blotting techniques. For cell membrane-bound or cell surface proteins, plasmon resonance is a more biologically relevant examination, even when performed on synthetic platforms, i.e., without cell membranes. Nevertheless, the interrogation of protein-protein interactions in real-time, in live cells, is more challenging due to the highly dynamic processes that occur spontaneously in uncontrolled and rapidly changing environments amidst the background of the cells' metabolism and systems biology. Whilst live-cell imaging approaches are useful in this regard, they are frequently limited to (i) the examination of a few hundred cultured adherent cells, (ii) the availability of fluorescent detection reagents that achieve sufficient signal-to-noise ratios permitting detection, and to (iii) susceptibility to phototoxicity effects where repeated light (or laser) interrogation induces cellular damage or where laser energies can ultimately disrupt chemical bonds in fluorophore structures (1,2). Flow cytometry represents a highly attractive approach to the investigation of protein-protein interactions, even for adherent cells that can be removed from the culture substrates. Indeed, if the molecules of interest emit a natural fluorescence, then they can be detected without the use of fluorescently conjugated antibodies or dyes. Additionally, almost any protein can be engineered to be expressed as a fluorescent fusion protein (3) or to contain naturally fluorescent amino acid epitope sequences such as the FlAsH (green) and ReAsH (red) tetracysteine-based epitope tags (4,5), thereby permitting their intrinsic detection without the use of antibodies or fluorescent dyes. This enables the careful and detailed examination of the fluorescent moiety for evidence of intra- or inter-molecular interactions by monitoring a number of effects on the fluorophore itself or changes in the fluorescent excitation and emission properties (3,6,7).

Green fluorescent protein (GFP) is a naturally arising fluorescent protein (FP), first described in the jellyfish *Aequorea Victoria* (8) but also found in a number of other organisms (9-11). Red fluorescent protein was similarly characterized from the *Discosoma* coral (DsRed). The molecular characterization of GFP has led to the careful strategic mutation of specific amino acids that alters the absorption, excitation and/or emission spectra of GFP (12,13). Cyan FP and yellow FPs or their enhanced versions ECFP and EYFP are molecular derivatives of GFP (7) (see FPbase: www.fpbase.org/protein/avgfp/), whereas monomeric RFP (mRFP) is derived from DsRed (14). The detection of naturally occurring fluorescence in these organisms can be utilized to monitor their existence and abundance and thereby the health of

ecosystems. However, these fluorescent proteins are now commonplace reagents within molecular biological investigations and as recombinant fluorescent fusion proteins. Furthermore, their biophysical properties have been well characterized including the photon absorption energy profiles, as well as their fluorescence excitation and emission profiles (14-16). More recently, fluorescent protein has been used in FRET-based applications. Fluorescence or Förster resonance energy transfer (FRET) is the phenomenon of non-radiative energy exchange between two (or more) component fluorescent entities (6,17). These can be chemically-linked single molecules, such as tandem dyes, for example, the PE-Cy7 fluorophore, or two (or more) extrinsic dyes within a single molecular entity with distinct fluorescence excitation/emission overlapping profiles for example Cy3/Cy5 (18), or chemically-linked fluorescent biosensor protein reagents (19-21). Alternatively, FRET can be achieved in unlinked but interacting molecular or protein multimers, such as two individual fluorescently-conjugated monoclonal antibodies (22), or two naturally fluorescent interacting proteins (23,24), or two synthetically expressed fluorescent fusion proteins (3), dependent upon the molecular distance between the fluorescent donor and acceptor elements within such interactions (FRET is a distinctly different phenomena from fluorescence complementarity techniques that monitor formation or disassociation of oligomeric fluorescent assembly). In this study, we utilize a model system comprising HEK293T cells transiently transfected with plasmids encoding fluorescent fusion protein of the TNFRSF and characterized their interactions by FRET cytometry.

Nascently expressed monomeric (type I) TNFRSF molecules spontaneously form dimers and trimers and oligomerize to transduce intracellular signaling pathways. When expressed as C-terminal fluorescence fusion proteins, the oligomerization state can be easily monitored. Here, we co-express TNFR1 as either a -CFP and -YFP FRET-1 pair, or as a -YFP and -RFP FRET-2 pair, or as a -CFP and -RFP FRET-3 pair, and as a negative control we co-express TNFR1 and CD27 fusion proteins (a non-TNFR1-interacting protein). This is therefore a chemically unlinked FRET reporter system for TNFR homotypic interactions. Elements of this system have been reported previously (3,25), but to date there are no broadly accepted standardization protocols for molecularly unlinked protein-protein interactions by FRET cytometry, and being molecularly unlinked system there are difficulties in how to measure FRET efficiency. For example, firstly, the donor and acceptor only -CFP, -YFP or -RFP single color controls for setting voltages can easily be generated by single plasmid transfections but there are no obvious single FRET channel positive controls (because this is a chemically unlinked FRET system). Secondly, detection of FRET is frequently only

determined after sample acquisition. Thirdly, to date no one has applied unsupervised multi-dimensional reduction analyses for unlinked FRET detection. Also, the concentration of the FRET donor and FRET acceptor proteins are not defined and hence must be estimated. Here, we have developed a systematic approach that provides multiple evidence of FRET positive events by (i) applying "spiked" single donor fluorescence cells to the sample prior to acquisition – to generate FRET channel histogram overlays visible during sample acquisition, (ii) including a non-FRETing molecular pair – to permit the analysis of concatenated data files and single-cell scatter distributions to visualize donor fluorescence loss, (iii) embracing uncompensated Phenograph analysis to rank FRET positive data, and (iv) using unsupervised multi-dimensional reduction analyses to confirm genuine FRET positive events. Despite being a chemically unlinked system, this method provides a strong evidence for FRET. Moreover, these approaches are clearly validated by the high degree of data similarity irrespective of sample acquisition on an LSR-II or Fortessa X-20 flow cytometer.

METHODS:

Generation of -CFP, -YFP and -RFP fusion protein expression plasmids. To generate TNFR1 and CD27 fusion proteins, pcDNA3 based plasmids were constructed. For pcDNA3.CD27-YFP the cDNA sequence of human CD27 was amplified from mRNA isolated from human peripheral blood mononuclear cells by RT- PCR (First Strand cDNA synthesis kit, Life Technologies) using PCR forward primer 5-'AGCAGGTACCATGGCACGGCCA CATCCCTGGTGG-3'and reverse primer 5'-TACTAACTCGAGGGGGGAGCAGGCAGG CTCCGGTT-3'. This introduces *KpnI* and *XhoI* restriction enzyme sites (underlined) into the PCR product. This enabled TNFR1 cDNA to be replaced with CD27 cDNA in pcDNA3.TNFR1-CFP and pcDNA3.TNFR1-YFP plasmids (kindly provided originally by Dr. F. Chan) (3). To generate pcDNA3.CD27-RFP and pcDNA3.TNFR1-RFP plasmids, monomeric RFP cDNA was PCR amplified from pVitro2-mRFP (generously provided by Dr Martiniello-Wilks, University of Technology Sydney) with RFP forward primer 5'-ATCCTCGAGATGGCCTCCTCCGAGGA-3' and a plasmid specific reverse primer 5'-AACCTGCTCCTAGGGTCGACAATCGAT-3' which contains a *XhoI* and *AvrII* (compatible with *XbaI*) restriction sites. Thus, the mRFP cDNA replaced YFP cDNA.

Plasmids Preparation. For large scale plasmid preparation, each pcDNA3-based plasmid was heat-shock transformed into the chemically competent *E. coli DH5α* bacterial cells (26), and a single colony was picked and incubated in LB at 37°C overnight. Plasmid DNA

isolation was performed by alkaline lysis (200mM NaOH, 1%SDS) of the bacterial cells and followed by neutralization with 4.2M Guanidine-HCl, 0.9M potassium acetate pH4.8. The sample was run through a silica column, washed with 10mM Tris-HCl pH7.5 in 80% ethanol and eluted in dH_2O (Sartorius). Potential endotoxin/LPS contamination was removed with Triton X-114 (27) and confirmed by LAL assay (Pierce).

HEK293T Cells and Transfection. Human embryonic kidney (HEK293T) cells (28) were the gift of Dr. Grant Logan (Children's Medical Research Institute, Australia). HEK293T cells were grown in Dulbecco's Modified Eagle medium (DMEM) supplemented with 10% heat-inactivated fetal bovine serum (FBS), 100U/ml penicillin and 100µg/ml streptomycin (all reagents from Life Technologies) at 37°C with 5% CO_2, and sub-cultured using 0.25% (w/v) Trypsin-0.53 mM EDTA solution (Life Technologies) for 5-10 minutes at 37°C, to detach from the plastic culture vessel. Cells were seeded into 6-well tissue culture dishes (Corning) at a concentration of 0.8×10^6 cells/mL in 2mls/well, 24 hr prior to transfection, and the media was replaced with fresh DMEM 2hr before transfection. A DNA mixture (solution A) containing a total of 4µg of plasmid DNA, plus 10µL of 2.5M $CaCl_2$ (Sigma-Aldrich) in a total volume of 100µL was prepared and added dropwise, with mixing, into FACS tube containing 100µL of 280mM NaCl, 1.5mM Na_2HPO_4, 50mM HEPES, 10mM KCl and 12mM D-Glucose (solution B, pH 7.05) and incubated for 20 min at room temperature. The precipitated DNA mixture was then pipetted evenly across the well of HEK293T cells, and the culture media was replaced with fresh DMEM 4hr later. Transfected cells were incubated for 48hr before examination.

Flow Cytometry and Data Acquisition. Single-cell suspensions of transfected HEK293T cells were prepared by gentle pipetting to detach cells from the plastic dish, and gauze-filtered (100µm pore size, Sefar) to remove any remaining cell clumps. Cells were centrifuged at 300×g for 5 min at 4°C and fixed in 0.5mL of freshly thawed 2% paraformaldehyde/PBS. Samples were divided into duplicate sets of FACS tubes and acquired on an LSR-II flow cytometer (Becton-Dickinson) equipped with UV 325nm (20mW), violet 405nm (25mW), blue 488nm (20mW) and red 640nm (20mW) lasers and a Fortessa X-20 flow cytometer (Becton-Dickinson) equipped with violet 405nm (50mW), blue 488nm (100mW) and red 640nm (40mW) lasers, on the same day.

The cytometry acquisition settings were as follows: first, a FSC-A/SSC-A dot plot was drawn to detect cells (R1) with the FSC threshold set at 5000, then a FSC-A/FSC-H dot plot was

used to define and gate on single cells (R2). Next, the unstained pcDNA3 empty vector transfected cells, and single-color controls (single transfections with CFP, YFP or RFP expression plasmids) were acquired and used to adjust the laser voltages and set the compensation values to minimize bleeding-through into adjacent channels (see Supplementary Figure 1). This is necessary due to the broad emission spectra of these fluorophores (Figure 1). The co-transfected cells were then examined using two parameter dot plots to define single donor FP (R3) and double-positive (CFP and YFP, or YFP and RFP, or CFP and RFP) co-transfected cells (R4) (Figure 2). Of note: the transfected cells were "spiked" with cells expressing the single donor fluorescent protein, immediately prior to acquisition on the cytometer, as this permitted: (i) the detection of single donor FP cells and (ii) careful adjustment of FRET detection channel (Figure 1) voltage settings. The amount of spiked cell events can be tailored to individual experimental needs, by adding more or less spiked cells. Therefore, both laser-excited donor cells and FRET-excited acceptor cell profiles are visualized in two-parameter dot-plots: for example, FRET-1/CFP (donor), and FRET-1/YFP (acceptor) etc. (Figure 1). Generally, 30,000 cells were collected using the FACS DIVA software (v8.0.2, Becton-Dickinson). FACS data were recorded and exported as FCS3.0 files.

Conventional Flow Cytometry Data Analysis. Data were analyzed using FlowJo (BD, v10.7.2). Briefly, the same dot-plots and gating strategy as described above were drawn in FlowJo, and compensation settings were checked and adjusted if needed using the Compensation workspace matrix. Histogram overlays of FRET detection channel data were generated with calculated geometric mean fluorescence intensity (MFI).

Concatenated Data Analysis. FRET emission channel data can also be compared by concatenating FRET positive (TNFR1+TNFR1) and FRET negative (TNFR1+CD27) transfected cell samples, then defining a gate that achieves equal laser-excited acceptor MFI values (black gated cells, see B, D, and F in Figures 2 and 3). These data are exported as .csv files and imported into Graphpad Prism (v8.4) to generate the frequency distribution scatter plots showing single cell fluorescent intensity. Alternatively, the frequency distribution scatter plots were also drawn from all data in R4 (color gated cells). A two-tailed unpaired t-test with Welch's correction was applied to define the statistically significance.

Single Cell FRET Efficiency Calculation. To calculate single cell FRET efficiency, first, the detection channel data were unmixed. For this, the background fluorescence was

corrected by subtracting the MFI of the autofluorescence from pcDNA3 empty plasmid transfected cells. Then, the bleed-through of each single background-corrected donor and acceptor fluorescence was determined using the following modifications of the following established method (20,29,30). First, a series of linear regression analyses were performed to determine the coefficient (slope relationship) between each possible pair of detection channels (Supplementary Figure 2). Next, a vector matrix *equation (1)* was used to calculate the unmixed donor $I_D(1\text{-}E)$, acceptor I_A, and FRET emissions $I_D E\alpha$, as follows.

$$\begin{bmatrix} I_D(1-E) \\ I_A \\ I_D E\alpha \end{bmatrix} = \begin{bmatrix} I_1 \\ I_3 \\ I_2 \end{bmatrix} \times \begin{bmatrix} 1 & S_4 & \frac{S_4}{S_2} \\ S_3 & 1 & \frac{1}{S_2}\frac{\varepsilon^D_{\lambda A}\varepsilon^A_{\lambda D}}{\varepsilon^D_{\lambda D}\varepsilon^A_{\lambda A}} \\ S_1 & S_2 & 1 \end{bmatrix}^{-1} \quad \textit{(Equation 1)}$$

Here, I_1, I_2 and I_3 are the donor, FRET, and acceptor fluorescence detected values before unmixing. For donor plasmid only transfected cells, S_1 is the coefficient between donor and FRET channels and S_3 is the coefficient between donor and acceptor channels. For acceptor plasmid only transfected cells, S_2 is the coefficient between acceptor and FRET channels and finally, S_4 is the coefficient between acceptor and donor channels. The extinction coefficient ε of the donor and acceptor fluorescent proteins can be found at the FPbase database (https://www.fpbase.org/) where λ is the donor and acceptor laser (nm wavelength). The α factor is calculated with *equation (2)* according to (20), with the assumption that the expression rate of the CFP-, YFP-, or RFP- fusion proteins (of the same molecule e.g., TNFR1) are highly similar. Thus, the concentration C_D and C_A offset or cancel out. It is acknowledged that in this chemically unlinked TNFR-FP model system a key assumption is that $C_D = C_A$ (or very close to this). This is based on the fact that both the donor and acceptor TNFR1-FP expression is driven by pcDNA3 plasmids containing the strong constitutive cytomegalovirus promoter sequences and plasmid 3'- mRNA elements, where the tRNA pool for protein expression is the same in all cells (HEK293T cells are a clonal cell line) where the plasmid DNA is carefully quantitated and mixed together before transfection. Alternatively, it remains, that C_D/C_A can perhaps be estimated by considering the cost function where we find that C_D/C_A is always quite close to 1 (Supplementary Methods and Supplementary Figure 3), even though data represents the average of all molecules expressed in each cell. Also, FRET positive pairs (TNFR1+TNFR1) and FRET negative pairs (TNFR1+CD27) are expected to have the same α value because the concentration and intensity terms will offset each other, as also shown in *equation 2*.

$$\alpha = \frac{I_3 S_2}{I_1}\frac{\varepsilon^D_{\lambda D} C_D}{\varepsilon^A_{\lambda D} C_A} \quad \textit{(Equation 2)}$$

Thus, the single cell FRET efficiency is expressed as 1 minus the donor emission (when exciting the FRET pair acceptor) divided by the donor emission (without exciting the FRET pair acceptor) as shown in *equation 3*.

$$E = 1 - \frac{I_{DA}}{I_D} = \frac{I_D - I_{DA}}{I_D} = \frac{I_D E}{I_D(1-E) + I_D E} \quad (Equation\ 3)$$

Using this method, the single cell FRET efficiencies were plotted with the matplotlib python library (matplotlib.pyplot.hist) with the bin size of 0.01 and the data distribution properties – mean, median, mode, SD and maximum were derived. In this molecularly unlinked FRET system, the comparison is between FRET positive cells (e.g., TNFR1-CFP+TNFR1-YFP) and FRET negative cells (e.g., TNFR1-CFP+CD27-YFP) but these profiles appear to overlap slightly. From a statistical perspective, it can be assumed that a meaningful positive FRET value, i.e., that is statistically significantly different, is by definition, any value greater than three standard deviations from the mean of the FRET negative sample. SDs are therefore also shown in the single cell FRET efficiency plots.

Clustering and Dimensionality Reduction Analysis. Linear scaled fluorescent intensity data were log transformed and then normalized based on the Z-score to achieve $\bar{x}$=0 and SD=1. For clustering, the Phenograph (version 1.5.2) python library was used with default settings and k=200 (31). For dimensionality reduction, five different methods were used. Briefly, t-SNE was performed using the scikit-learn (version 0.24.2): sklearn.manifold.TNSE library with perplexity=200, early_exaggeration=5, learning rate=200, number of iterations=500, metric=Euclidean, method=barnes_hut and angle=0.3 (32). Fit-SNE was performed using the openTSNE (version 0.6.0) python library, with perplexity=50, exaggeration=5, metric=Euclidean, learning rate=200 and theta=0.3 (33). UMAP was performed with the umap-learn (version 0.5.1) python library with number of neighbors=100, minimum distance=0.4 and metric=Euclidean (34). Tri-MAP was performed with the Tri-MAP (version 1.0.15) python library with number of inliers=100, number of outliers=10, learning rate=200, distance=Euclidean and number of iterations=500 (35). For PaCMAP, the pacmap (version 0.5.2) python library was used with number of neighbors=100, medium near ratio=0.3, far point ratio=2 and learning rate=0.1 (36). The FRET positive dimensionality reduction visualizations shown in color (C→Y FRET1: green, Y→R FRET2: orange, C→R FRET3: purple, or with multicolor ranked clusters) were simultaneously determined with FRET negative cells (grey). The ranked clusters (highest to lowest) were determined based on the single FRET efficiency calculations.

RESULTS

Establishing FRET detection channels. To consider the LSR-II and Fortessa X-20 cytometer instrument potential for the detection of -CFP, -YFP, -RFP fusion proteins simultaneous with C→Y (FRET-1), Y→R (FRET-2) and C→R (FRET-3) emission signals, cytometer laser and filter configurations were assessed. Both instruments have lasers and detectors appropriate for the detection of conventional fluorescent proteins CFP, YFP and RFP (Table 1). CFP is excited and detected by the 405nm laser (450/50nm BP filter) and YFP by the 488nm laser (530/30nm on LSR-II and 542/27nm on Fortessa X-20) (Figure 1). Although RFP is often optimally excited by a yellow green 561nm laser, not all the older cytometers have this laser. Instead, RFP can be excited and detected by a 488nm laser (670/14nm on LSR-II and 695/40nm on Fortessa X-20) (Figure 1). FRET fluorescence needs to be carefully aligned to the laser that excites the donor fluorescent molecule. In this case, C→Y (FRET-1) and C→R (FRET-3) emission signals are positioned within the 405nm detector array for both LSR-II and Fortessa X-20 cytometers (Figure 1 and Table 1). FRET-1 fluorescence is detected with a narrow BP filter (546/10nm for LSR-II and 540/10nm for Fortessa X-20) positioned immediately after the CFP emission signal (which in this case acts as the FRET-1 donor), and FRET-3 fluorescence is detected (610/20nm) also after CFP, because CFP is also the donor in this FRET pair (Figure 1 and Table 1). Similarly, Y→R (FRET-2) excitation is positioned on the 488nm laser detector array, because YFP is the FRET-2 donor molecule, where FRET-2 is detected at 610/20nm on both LSR-II and Fortessa X-20 cytometers.

FRET Signal Detection During Sample Acquisition. In conventional flow cytometry, single color controls are essential for setting the voltage and compensation values, although FRET cytometry analysis is often performed with inadequate compensation (37-39). The value of using compensation, however, is to visualize two-molecule FRET emission during acquisition. Therefore, single color controls were used to set the voltage and compensation for CFP, YFP, RFP and C→Y (FRET-1), Y→R (FRET-2) and C→R (FRET-3) (Supplementary Figure 1 and Figure 2 and 3 A, C and E). In our system, these fluorescent proteins are expressed in transfected HEK293T cells as TNFR-superfamily fusion proteins TNFR1-CFP, TNFR1-YFP, TNFR1-RFP or CD27-fusion proteins. The FRET-1, -2, and -3 emissions are thereby easily visualized in two-parameter dot-plots in co-transfected cells, versus the CFP, YFP or RFP emissions (Figure 2 and 3, A, C and E), gating first on single cells (FSC-A/SSC-A, R1, then FSC-A/FSC-H, R2, data not shown). Furthermore, the FRET signal is clearest when directly compared to the donor fluorescence alone, and hence the samples were manually “spiked” with single donor fluorescence TNFR1 transfected cells, immediately prior

to sample acquisition (Figure 2 and 3 A, C and E). This approach permits direct visualization in histogram overlays of FRET emission from the single donor cells (R3), and co-transfected cells (R4) during sample acquisition. In fact, the FRET MFI of TNFR1+TNFR1 co-transfected cells was always consistently significantly higher than that in TNFR1+CD27 co-transfected cells (Figure 2 and 3 A, C and E).

The two data files of TNFR1+TNFR1, and TNFR1+CD27 samples, can be concatenated and analyzed in single scatter plots, which provided further evidence of the relative loss of the donor fluorescence as an indicator of FRET activity (Figure 2 and 3 B, D and F). For example, reduced CFP in C→Y FRET-1, reduced YFP in Y→R FRET-2, or reduced CFP in C→R FRET-3 indicates that genuine FRET energy transfer has occurred. Also, concatenated data allows for gating on cells with the same acceptor MFI level (black events). In all cases, TNFR1+TNFR1 co-expression resulted in a loss of donor fluorescence, relative to TNFR1+CD27, consistent with TNFR1 forming donor-acceptor FRET pairs (Figure 2 and 3 B, D and F). Both conventional or concatenated data appear similar irrespective of whether the samples were acquired on an LSR-II cytometer or a Fortessa X-20 cytometer - compare Figures 2 and 3.

Calculated Single Cell FRET Efficiency and Multi-dimensional Reduction Analyses. In this chemically unlinked FRET system analyzing TNFR monomer interactions, FRET-1, FRET-2 and FRET-3 efficiency can be calculated on a single cell uncompensated basis because the following factors can be determined for every cell event: I_1, I_2, I_3, S_1, S_2, S_3, S_4, ε, λ and α (see method for definitions). Single cell FRET efficiencies were therefore calculated and plotted (bin size=0.01) for both TNFR1+TNFR1 (FRET positive) and TNFR1+CD27 (FRET negative) co-transfected cells (Figure 4 A, C and E). For TNFR1+TNFR1 transfected cells, the C→Y FRET-1 efficiency for was determined to be 0.43 (LSR-II) or 0.41 (Fortessa X-20), and the Y→R FRET-2 efficiency was 0.30 (LSR-II) or 0.29 (Fortessa X-20), whilst the C→R FRET-3 efficiency was 0.56 (LSR-II) or 0.54 (Fortessa X-20). As expected, all TNFR1+CD27 (FRET negative) co-transfected cells yielded FRET efficiencies closer to zero, despite the chance of non-specific or "by chance" interactions. In fact, all of the distribution and modal characteristics of the FRET efficiency data were quite similar irrespective of whether the samples were acquired on the LSR-II or Fortessa X-20 (Table 2), as were the estimated molecular distances of the interacting TNFR1-FP FRET-pairs (Supplementary Figure 4).

Single cell FRET efficiency data was also interrogated using Phenograph. This permitted discrimination of 7 clusters based on FRET efficiencies (colored heatmaps), and these were aligned to the donor, acceptor, and FRET emission channel data (grey heatmaps) (Figure 4 B, D and F). These data further confirmed the detection of TNFR1+TNFR1 (FRET positive) event signals compare to TNFR1+CD27 (FRET negative) events. These data also explain FRET efficiency data overlaps, most evident for C→Y FRET-1 compared to Y→R FRET-2 and C→R FRET-3. In conclusion, these analyses indicate that C→R FRET-3 FRET-pair yields the highest FRET efficiency and the best separation between FRET positive and FRET negative events (Figure 4 and Table 2). Thus, even in this chemically unlinked TNFR fusion protein system, it is evident that FRET efficiency calculated at a single cell level provides strong evidence of FRET activity between fluorescent TNFR monomers. Nevertheless, utilizing the donor, acceptor and FRET detection channel data for each FRET pair, multi-dimensional reduction analyses by t-SNE, Fit-SNE, UMAP, Tri-MAP and PaCMAP (33-35,40) also efficiently separated the TNFR1+TNFR1 (FRET positive, green, orange or purple) events from the TNFR1+CD27 (FRET negative, grey) events. Thus, irrespective of the focus of the algorithms, that is, t-SNE, Fit-SNE and UMAP emphasize local structure, Tri-MAP emphasizes global structure, and PaCMAP emphasizes both local and global structures of the data, the FRET positive events are distinguished from FRET negative events without considering FRET efficiency. Taken together, uncompensated analyses and FRET efficiency calculations confirm two molecule C→Y FRET-1, Y→R FRET-2 and C→R FRET-3 detections using a BD LSR-II or Fortessa X-20 cytometer even without a 561nm laser that is present in more recent instruments.

DISCUSSION.

The first obvious consideration of any FRET cytometry experiment is the number of the lasers and their wavelength (nm), second only to the number of detectors and their relative positions within detector arrays. The older LSR-II design requires separate long pass (LP) and band pass (BP) filters position immediately before the PMT detectors, whereas the newer Fortessa X-20 style instrument utilize an integrated LP/BP filter unit. Each of the 3 individual FRET pairs, C→Y FRET-1, Y→R FRET-2 and C→R FRET-3, were examined using transfected cells acquired on both a 4-laser LSR-II (355nm UV, 405nm violet, 488nm blue, and 640nm red) and a 3-laser Fortessa X-20 (405nm violet, 488nm blue, and 640nm red) as shown (Figure 1 and Table 1). Note that neither of these instruments contains a 561nm laser – optimal for RFP excitation, which is not necessary in this TNFR fusion protein system because (i) RFP FRET signal is detected on the same laser detector array as the donor FP, and

(ii) RFP can be sufficiently excited by the 488nm laser. Detection of CFP and YFP was straightforward utilizing standard filters, but the detection of the YFP FRET-1 emission requires a special order of 546/10nm (LSR-II) or 540/10nm (Fortessa X-20) narrow BP filter, due to the extensive overlap of CFP and YFP emission curves (Figure 1). Furthermore, in most examples of FRET cytometry, the donor and FRET emissions are positioned on the same detector array, and where the laser excited acceptor is detected separately – on a separate laser/detector array (20,25,41), see Table 1). This is true, for the FRET-1 and FRET-3 TNFR fusion protein systems used here. However, for both the LSRII and the Fortessa, the Y→R FRET-2 FRET pair (donor, acceptor, and FRET-2 emission) are detected on the same laser detector array, simply because RFP is excitable by the 488nm laser, and because neither instrument has a 561nm laser. If available, a 561nm laser would more efficiently excite the RFP (14), achieve lower variance in the calculated FRET efficiency, and in fact it is required to determine the FRET efficiency in FRET pairs where RFP is the FRET acceptor, because in the original published FRET efficiency calculations, three separate equations are required (for the donor, acceptor and FRET intensities)(29) and the capacity to excite the acceptor and measure its emission intensity separate from FRET excitation. Instead, by applying a matrix calculation (see methods), we have directly solved the unmixed donor $I_D(1\text{-}E)$, acceptor I_A, and FRET $I_D E\alpha$ emissions, and the FRET efficiency (E) is then determined with the α factor irrespective of the use of single laser for RFP (acceptor) and FRET-2 – achieved by two filter sets spatially separate but both aligned within the RFP emission spectrum (Figure 1). Also, taken on face value, whilst it might appear that there is greater precision of measurement of FRET efficiency in the yellow-red detection than the green regimes but this may simply be an artefact of autofluorescence of HEK293T cells, even though cell endogenous autofluorescence is considered through the inclusion of pcDNA3 empty vector transfected cells.

ECFP and EYFP are molecular derivatives of the original jellyfish *Aequorea Victoria* GFP (8), the red fluorescent protein used here is actually monomeric RFP derived from DsRFP from *Discosoma* coral (14), and this is essential because FRET pairs must be monomers. Whilst nascently expressed TNFR-fusion proteins are monomers, TNFRs structurally form dimers or trimers that oligomerize after engagement with ligand (42-44). Overexpression of TNFRs is sufficient for TNFR function and signaling (45-47) and hence transfected HEK293T cells would be expected to express a wide array of TNFR molecule complexes: dimers and even trimers. In fact, the dimers and trimers will comprise both homo- and hetero-dimers, i.e., with endogenous receptors and/or fluorescent fusion proteins, e.g., CFP::CFP,

YFP::YFP, or CFP::YFP and hetero- and homo-trimers even on a single cell. This feature of the TNFR1 biology means that homo-FRET, comprised for example of TNFR1-CFP::TNFR1-CFP, is a component of this system. If so, then the CFP is detected within the CFP channel, and any hetero-FRET must necessarily involve cross-dimer FRET which is expected to be less efficient than a true TNFR1-CFP::TNFR1-YFP heterodimer FRET. In the case of TNFR1+CD27 co-transfected cells no FRET signals are expected because TNFR1 and CD27 do not biochemically or physically form heterocomplexes, except due the chance of non-specific interactions. Instead, these cells can only express homo- dimeric or trimeric molecular forms of TNFR1 molecules. Since FRET emission only occurs when two fluorescent molecules are in sufficiently close proximity to permit the excited state energy transfer ($\leq$100Å or $\leq$10nm (17)), and only TNFR1+TNFR1 transfected cells should lead to sensitized emission / FRET signal / FRET intensity, even though TNFR1-FPs and CD27-FPs could theoretically be sufficiently close simply by a chance non-specific interaction and therein produce a FRET emission. Here, the FRET efficiency data can be interpreted to yield information about the molecular distance (nm) between TNFR1-FP dimers, which range from 0.40 to 0.45nm for TNFR1-CFP:TNFR1-YFP, to 0.62 to 0.65 nm for TNFR1-YFP:TNFR1-RFP, and 0.44 to 0.45 nm for TNFR1-CPR:TNFR1-RFP (Supplementary data Table and Supplementary Figure 4), where the differences may reflect the differences in CFP/YFP and RFP fluorophore structures or the instrument precision/filter options and efficiency of fluorescence intensity detection. Nevertheless, this paper describes multiple evidence for genuine two molecule FRET emission, including (i) visualizing single donor "spiked" cells and co-transfected cells during sample acquisition, (ii) simple FRET channel emission MFI overlays, (iii) concatenated data examined as single cell scatter plots, (iv) single cell FRET efficiency calculation, (v) multi-dimensional reduction data analyses. All of these analyses produce data where TNFR1+TNFR1 can be discriminated from TNFR1+CD27 transfected cells. Arguably, the most robust indicator of FRET is generated by calculating FRET efficiency, nevertheless of multi-dimensional reduction analyses of uncompensated donor, acceptor and FRET emission data also produced unequivocal evidence of FRET positive cells visually separate from FRET negative cells. The broad distribution of calculated two molecule FRET efficiency correlates with the Phenograph analysis (ranked clusters), and likely demonstrates structural complexity and natural biological roles of TNFRs. Whilst we clearly demonstrated two molecule FRET, others have already reported using tripleFRET with three fluorophore conjugated monoclonal antibodies (48) or a linked fluorophore system (38), we are therefore currently focusing on standardizing TNFR-fusion protein tripleFRET.

In summary, the data presented here clearly demonstrates 3 individual two-molecule FRET pairs (C→Y FRET-1, Y→R FRET-2 and C→R FRET-3) in a chemically unlinked biologically relevant cell-based system. The calculated single-cell two molecule FRET efficiency data produced highly similar profiles of FRET (Figure 4 and Table 2) irrespective of the cytometer used or the age of the instrument (the LSR-II was purchased in 2007, and Fortessa was purchased in 2014). Therefore, this paper demonstrates robust detection of non-chemically linked FRET representing TNFRSF structures with high precision, including the capacity to monitor the likely FRET signal detection during sample acquisition.

CONCLUSIONS:

This paper describes a comprehensive method for FRET detection by conventional flow cytometry examining three individual FRET pairs and two different flow cytometers. We document the step-by-step process for comparing FRET positive and FRET negative cells simultaneous with "spiked" donor fluorescent positive cells during sample acquisition. The C→Y FRET-1, Y→R FRET-2 and C→R FRET-3 signals are viewed together with donor and acceptor fluorescence compensated by single color controls and subsequentially analyzed uncompensated for FRET efficiency calculation and via multidimensional reduction analyses. When comparing each of the FRET pairs and all these analyses, it is clear that flow cytometry FRET emission can be reliably detected in molecules that are known to form homo-multimers - but not so in those molecules that do not biochemically physically associate. Moreover, the differences in the FRET efficiency profiles comparing C→Y FRET-1, to Y→R FRET-2 or C→R FRET-3, can be used to choose which FRET pair might most optimally be used for any given FRET cytometry application. Furthermore, the data presented here indicate close precision between cytometer instruments despite large differences in age or laser and bandpass filter configurations. This approach confirms the capacity to visualize simultaneously with sample acquisition and validated by robust mathematical calculations of single cell FRET efficiency. Thus, the separation of the FRET positive signals from the FRET negative signals are unambiguously achieved with and without compensation-based approaches.

ACKNOWLEDGEMENTS.

The authors thank Dr Chan for the TNFR1 plasmid and Dr Martiniello-Wilks for an mRFP cDNA (plasmid DNA). ZN is a PhD student at UTS supported by a UTS International Research Scholarship and a UTS President's Scholarship. Author ZN also acknowledges sustained support from Ms Kerui Xu. LMS acknowledges the support of a UTS Equity and

Re-Establishment Grant.

AUTHOR CONTRIBUTION STATEMENT.

ZN, AG and LMS constructed plasmid reagents.

ZN, AG, and LMS designed the experiments.

ZN and LMS performed the experiments.

ZN and LMS analyzed and interpreted the data.

ZN and LMS prepared the paper figures.

MSJ and LMS supervised the project.

ZN and LMS co-wrote the paper.

Table 1: Cytometer Configurations for FRET.

LSRII				
Laser	**Position**	**LP Filter (nm)**	**BP Filter (nm)**	**Signal Detected**
355nm (20mW)	A	505LP	530/30	Available
	B	410LP	450/50	Available
	C	-	379/28	Available
405nm (20mW)	A	595LP	610/20	RFP (FRET-3)
	B	500LP	546/10	YFP (FRET-1)
	C	-	450/50	CFP
488nm (20mW)	A	735LP	780/60	Available
	B	685LP	695/40	Available
	C	635LP	670/14	RFP
	D	595LP	610/20	RFP (FRET-2)
	E	500LP	530/30	YFP
	F	-	488/10	SSC
	G	Empty	Empty	(No PMT)
640nm (20mW)	A	735LP	780/60	Available
	B	710LP	730/45	Available
	C	-	660/20	Available
Fortessa X20				
Laser	**Position**	**Integrated Filter Unit[1] LP / BP (nm)**		**Signal Detected**
405nm (50mW)	A	750LP	780/60	Available
	B	690LP	710/50	Available
	C	635LP	670/30	Available
	D	600LP	610/20	RFP (FRET-3)
	E	505LP	540/10	YFP (FRET-1)
	F	-	450/50	CFP
	G	Empty		(No PMT)
	H	Empty		(No PMT)
488nm (100mW)	A	750LP	780/60	Available
	B	635LP	695/40	RFP
	C	600LP	610/20	RFP (FRET-2)
	D	550LP	575/25	Available
	E	505LP	542/27	YFP
	F	-	488/10	SSC
	G	Empty		(No PMT)
	H	Empty		(No PMT)
640nm (40mW)	A	750LP	780/60	Available
	B	710LP	730/45	Available
	C	-	670/14	Available
	D	Empty		(No PMT)
	E	Empty		(No PMT)
	F	Empty		(No PMT)
	G	Empty		(No PMT)
	H	Empty		(No PMT)

Table 2. Instrument comparison of FRET efficiency.

	LSR-II	Fortessa X-20	LSR-II	Fortessa X-20
FRET1 C→Y	FRET1+$_E$ R1+R1	FRET1+$_E$ R1+R1	FRET1-$_E$ R1+CD27	FRET1-$_E$ R1+CD27
Mean	0.43	0.41	0.08	0.07
SD	0.17	0.20	0.11	0.10
Median	0.45	0.42	0.00	0.00
Mode	0.46	0.48	0.00	0.00
Maximum	0.71	0.77	0.46	0.40
FRET2 Y→R	FRET2+$_E$ R1+R1	FRET2+$_E$ R1+R1	FRET2-$_E$ R1+CD27	FRET2-$_E$ R1+CD27
Mean	0.30	0.29	0.02	0.03
SD	0.12	0.09	0.03	0.06
Median	0.30	0.31	0.00	0.00
Mode	0.35	0.31	0.00	0.00
Maximum	0.71	0.65	0.14	0.14
FRET3 C→R	FRET3+$_E$ R1+R1	FRET3+$_E$ R1+R1	FRET3-$_E$ R1+CD27	FRET3-$_E$ R1+CD27
Mean	0.56	0.54	0.02	0.02
SD	0.16	0.13	0.04	0.03
Median	0.60	0.56	0.00	0.00
Mode	0.62	0.56	0.00	0.00
Maximum	0.95	0.72	0.50	0.21

FIGURE LEGENDS.

Figure 1. Spectral viewer profiles of detection of CFP, YFP, RFP, and FRET channels. Spectral profiles and detector parameters are shown for both an LSR-II **(A)** and a Fortessa X-20 flow cytometer **(B)**. Excitation and emission profiles of CFP, YFP and RFP, indicating lasers (nm) for excitation, and bandpass filters (nm) for detection. FRET pair excitation and emission spectra are also shown, again indicating lasers used for FRET donor excitation, and filters bandpass width and detector array positions for FRET detection.

Figure 2. FRET Pair Emission Data: C→Y FRET-1, Y→R FRET-2 and C→R FRET-3 (LSR-II). TNFR1+TNFR1 compared to TNFR1+CD27 emission data in co-transfected HEK293T cells. Donor acceptor 2 parameter dot-plot are shown along with donor or acceptor versus FRET, and histogram overlays (plus geometric MFI) of double positive (R4) versus single positive donor "spiked" (R3) **(A, C and E)**. Concatenated dot plot analysis showing TNFR1+TNFR1 together with TNFR1+CD27 co-transfected cell cultures **(B, D and F)**, together with frequency distribution scatter plots showing FRET donor, acceptor, and FRET channel fluorescence data. Data is shown, first for all events in R4 gate (colour), and second for only those events that have the equal FRET acceptor geometric MFI value (black). The geometric mean (black or grey bar) is determined from the R4 gated events in the concatenated dot plot, and statistical significance (t-test) is indicated *** $p<0.001$.

Figure 3. FRET Pair Emission Data: C→Y FRET-1, Y→R FRET-2 and C→R FRET-3 (Fortessa X-20). TNFR1+TNFR1 compared to TNFR1+CD27 emission data in co-transfected HEK293T cells. Donor acceptor 2 parameter dot-plot are shown along with donor or acceptor versus FRET, and histogram overlays (plus geometric MFI) of double positive (R4) versus single positive donor "spiked" (R3) **(A, C and E).** Concatenated dot plot analysis showing TNFR1+TNFR1 together with TNFR1+CD27 co-transfected cell cultures **(B, D and F)**, together with frequency distribution scatter plots showing FRET donor, acceptor, and FRET channel fluorescence data. Data is shown, first for all events in R4 gate (colour), and second for only those events that have the equal FRET acceptor geometric MFI value (black). The geometric mean (black or grey bar) is determined from the R4 gated events in the concatenated dot plot, and statistical significance (t-test) is indicated *** $p<0.001$.

Figure 4. FRET pair data analysis for C→Y FRET-1, Y→R FRET-2 and C→R FRET-3. Single cell FRET efficiencies were calculated (see methods) and plotted as binned data (bin size 0.01) to illustrate the full distribution of FRET efficiency per cell using data obtained on both an LSR-II and a Fortessa X-20 flow cytometer from a single representative experiment using transfected HEK293T cells. Single cell FRET efficiency data for either TNFR1+TNFR1 or TNFR1+CD27 transfected cells were used to calculate an average ($\bar{x}$) FRET efficiency for each FRET pair **(A, C and E)**. The standard deviation (+1SD, +2SD, +3SD) of the mean for the TNFR1+CD27 transfected FRET negative cells are also indicated. Heat maps show ranked clusters of calculated FRET efficiencies (colour; 7 groups determined using Phenograph with k=200), alongside donor, acceptor and FRET detection channel data (grey scale) for either TNFR1+TNFR1 or TNFR1+CD27 transfected cells **(B, D and F)**. Multidimension (donor, acceptor, and FRET channel intensity data) reduction maps were generated using t-SNE, Fit-SNE, UMAP, TriMAP and PaCMAP; data shown are TNFR1+TNFR1 FRET positive cell data (green, orange and purple, or calculated FRET clusters in multicolour) versus TNFR1+CD27 FRET negative cell data (grey).

LITERATURE CITED.

1. Daddysman MK, Tycon MA, Fecko CJ. Photoinduced damage resulting from fluorescence imaging of live cells. *Methods Mol Biol.* 2014; 1148: 1-17.
2. Song L, Hennink EJ, Young IT, Tanke HJ. Photobleaching kinetics of fluorescein in quantitative fluorescence microscopy. *Biophys J.* 1995; 68: 2588-2600.
3. Chan FK, Chun HJ, Zheng L, Siegel RM, Bui KL, Lenardo MJ. A domain in TNF receptors that mediates ligand-independent receptor assembly and signaling. *Science.* 2000; 288: 2351-2354.
4. Griffin BA, Adams SR, Tsien RY. Specific covalent labeling of recombinant protein molecules inside live cells. *Science.* 1998; 281: 269-272.
5. Adams SR, Tsien RY. Preparation of the membrane-permeant biarsenicals FlAsH-EDT 2 and ReAsH-EDT 2 for fluorescent labeling of tetracysteine-tagged proteins. *Nature Protocols.* 2008; 3: 1527-1534.
6. Selvin PR. Fluorescence resonance energy transfer. *Methods Enzymol.* 1995; 246: 300-34.
7. Miyawaki A, Llopis J, Heim R, McCaffery JM, Adams JA, Ikura M, Tsien RY. Fluorescent indicators for Ca2+ based on green fluorescent proteins and calmodulin. *Nature.* 1997; 388: 882-887.
8. Tsien RY. The green fluorescent protein. *Annu Rev Biochem.* 1998; 67: 509-544.
9. Stafford WF, Jacobsen MP, Woodhead J, Craig R, O'Neall-Hennessey E, Szent-Gyorgyi AG. Calcium-dependent structural changes in scallop heavy meromyosin. *J Mol Biol.* 2001; 307: 137-147.
10. Loening AM, Fenn TD, Gambhir SS. Crystal structures of the luciferase and green fluorescent protein from Renilla reniformis. *J Mol Biol.* 2007; 374: 1017-1028.
11. Jones AM, Ehrhardt DW, Frommer WB. A never ending race for new and improved fluorescent proteins. *BMC Biol.* 2012; 10: 39.
12. Nguyen AW, Daugherty PS. Evolutionary optimization of fluorescent proteins for intracellular FRET. *Nat Biotechnol.* 2005; 23: 355-360.
13. Davidson MW, Campbell RE. Engineered fluorescent proteins: innovations and applications. *Nat Methods.* 2009; 6: 713-717.
14. Campbell RE, Tour O, Palmer AE, Steinbach PA, Baird GS, Zacharias DA, Tsien RY. A monomeric red fluorescent protein. *Proc Natl Acad Sci USA.* 2002; 99: 7877-7882.
15. Heim R, Tsien RY. Engineering green fluorescent protein for improved brightness, longer wavelengths and fluorescence resonance energy transfer. *Curr Biol.* 1996; 6: 178-182.
16. Kremers GJ, Goedhart J, van Munster EB, Gadella TW, Jr. Cyan and yellow super fluorescent proteins with improved brightness, protein folding, and FRET Forster radius. *Biochemistry.* 2006; 45: 6570-6580.
17. Stryer L, Haugland RP. Energy transfer: a spectroscopic ruler. *Proc Natl Acad Sci USA.* 1967; 58: 719-726.
18. Roy R, Hohng S, Ha T. A practical guide to single-molecule FRET. *Nature methods.* 2008; 5: 507-516.
19. Jones DM, Padilla-Parra S. Imaging real-time HIV-1 virion fusion with FRET-based biosensors. *Scientific reports.* 2015; 5: 1-10.
20. Nagy P, Bene L, Hyun WC, Vereb G, Braun M, Antz C, Paysan J, Damjanovich S, Park JW, Szollosi J. Novel calibration method for flow cytometric fluorescence resonance energy transfer measurements between visible fluorescent proteins. *Cytometry A.* 2005; 67: 86-96.
21. Bajar BT, Wang ES, Zhang S, Lin MZ, Chu J. A guide to fluorescent protein FRET pairs. *Sensors.* 2016; 16: 1488.
22. Konig P, Krasteva G, Tag C, Konig IR, Arens C, Kummer W. FRET-CLSM and double-labeling indirect immunofluorescence to detect close association of proteins in tissue sections. *Lab Invest.* 2006; 86: 853-864.

23. Kofoed EM, Guerbadot M, Schaufele F. Dimerization between aequorea fluorescent proteins does not affect interaction between tagged estrogen receptors in living cells. *J Biomed Opt.* 2008; 13(3): 031207.
24. Ohashi T, Galiacy SD, Briscoe G, Erickson HP. An experimental study of GFP-based FRET with application to intrinsically unstructured proteins. *Protein Sci.* 2007; 16: 1429-1238.
25. Lo CH, Vunnam N, Lewis AK, Chiu TL, Brummel BE, Schaaf TM, Grant BD, Bawaskar P, Thomas DD, Sachs JN. An innovative high-throughput screening approach for discovery of small molecules that inhibit TNF receptors. *SLAS Discov.* 2017; 22: 950-961.
26. Inoue H, Nojima H, Okayama H. High efficiency transformation of Escherichia coli with plasmids. *Gene.* 1990; 96: 23-28.
27. Ma R, Zhao J, Du HC, Tian S, Li LW. Removing endotoxin from plasmid samples by Triton X-114 isothermal extraction. *Anal Biochem.* 2012; 424: 124-126.
28. Graham FL, Smiley J, Russell WC, Nairn R. Characteristics of a human cell line transformed by DNA from human adenovirus type 5. *J Gen Virol.* 1977; 36: 59-74.
29. Ujlaky-Nagy L, Nagy P, Szollosi J, Vereb G. Flow cytometric FRET analysis of protein interactions. *Methods Mol Biol.* 2018; 1678: 393-419.
30. Tron L, Szollosi J, Damjanovich S, Helliwell SH, Arndt-Jovin DJ, Jovin TM. Flow cytometric measurement of fluorescence resonance energy transfer on cell surfaces. Quantitative evaluation of the transfer efficiency on a cell-by-cell basis. *Biophys J.* 1984; 45: 939-946.
31. Levine JH, Simonds EF, Bendall SC, Davis KL, Amir el AD, Tadmor MD, Litvin O, Fienberg HG, Jager A, Zunder ER and others. Data-driven phenotypic dissection of AML reveals progenitor-like cells that correlate with prognosis. *Cell.* 2015; 162: 184-197.
32. Van der Maaten L, Hinton G. Visualizing data using t-SNE. *J Mach Learn Res.* 2008; 9.
33. Linderman GC, Rachh M, Hoskins JG, Steinerberger S, Kluger Y. Fast interpolation-based t-SNE for improved visualization of single-cell RNA-seq data. *Nat Methods.* 2019; 16: 243-245.
34. McInnes L, Healy J, Saul N, Großberger L. UMAP: uniform manifold approximation and projection. *J Open Source Softw.* 2018; 3: 861.
35. Amid E, Warmuth MK. TriMap: Large-scale dimensionality reduction using triplets. *arXiv preprint arXiv:1910.00204.* 2019.
36. Wang Y, Huang H, Rudin C, Shaposhnik Y. Understanding how dimension reduction tools work: an empirical approach to deciphering t-SNE, UMAP, TriMAP, and PaCMAP for data visualization. *arXiv preprint arXiv:2012.04456.* 2020.
37. Banning C, Votteler J, Hoffmann D, Koppensteiner H, Warmer M, Reimer R, Kirchhoff F, Schubert U, Hauber J, Schindler M. A flow cytometry-based FRET assay to identify and analyse protein-protein interactions in living cells. *PLoS One.* 2010; 5: e9344.
38. He L, Wu X, Simone J, Hewgill D, Lipsky PE. Determination of tumor necrosis factor receptor-associated factor trimerization in living cells by CFP->YFP->mRFP FRET detected by flow cytometry. *Nucleic Acids Res.* 2005; 33: e61.
39. He L, Olson DP, Wu X, Karpova TS, McNally JG, Lipsky PE. A flow cytometric method to detect protein-protein interaction in living cells by directly visualizing donor fluorophore quenching during CFP-->YFP fluorescence resonance energy transfer (FRET). *Cytometry A.* 2003; 55: 71-85.
40. Belkina AC, Ciccolella CO, Anno R, Halpert R, Spidlen J, Snyder-Cappione JE. Automated optimized parameters for T-distributed stochastic neighbor embedding improve visualization and analysis of large datasets. *Nat Commun.* 2019; 10: 5415.
41. Chan FK, Holmes KL. Flow cytometric analysis of fluorescence resonance energy transfer: a tool for high-throughput screening of molecular interactions in living cells. *Methods Mol Biol.* 2004; 263: 281-292.

42. Naismith JH, Devine TQ, Brandhuber BJ, Sprang SR. Crystallographic evidence for dimerization of unliganded tumor necrosis factor receptor. *J Biol Chem.* 1995; 270: 13303-13307.
43. D'Arcy A, Banner DW, Janes W, Winkler FK, Loetscher H, Schonfeld HJ, Zulauf M, Gentz R, Lesslauer W. Crystallization and preliminary crystallographic analysis of a TNF-beta-55 kDa TNF receptor complex. *J Mol Biol.* 1993; 229: 555-557.
44. Schneider-Brachert W, Tchikov V, Neumeyer J, Jakob M, Winoto-Morbach S, Held-Feindt J, Heinrich M, Merkel O, Ehrenschwender M, Adam D and others. Compartmentalization of TNF receptor 1 signaling: internalized TNF receptosomes as death signaling vesicles. *Immunity.* 2004; 21: 415-428.
45. Hayder H, Blanden RV, Körner H, Riminton DS, Sedgwick JD, Müllbacher A. Adenovirus-induced liver pathology is mediated through TNF receptors I and II but is independent of TNF or lymphotoxin. *J Immunol.* 1999; 163: 1516-1520.
46. Sedger LM, Osvath SR, Xu XM, Li G, Chan FK, Barrett JW, McFadden G. Poxvirus tumor necrosis factor receptor (TNFR)-like T2 proteins contain a conserved preligand assembly domain that inhibits cellular TNFR1-induced cell death. *J Virol.* 2006; 80: 9300-9309.
47. Sedger LM, Shows DM, Blanton RA, Peschon JJ, Goodwin RG, Cosman D, Wiley SR. IFN-gamma mediates a novel antiviral activity through dynamic modulation of TRAIL and TRAIL receptor expression. *J Immunol.* 1999; 163: 920-926.
48. Fábián Á, Horvath G, Vamosi G, Vereb G, Szollosi J. TripleFRET measurements in flow cytometry. *Cytometry A.* 2013; 83: 375-385.

Supplementary Methods.

To better consider the concentration C of the FRET donor (C_D) and FRET acceptor (C_A) proteins there are two options. First, one can consider *approach 1*, as shown below:

$$R_F = \frac{F_{AD}}{F_A} = 1 + \frac{\varepsilon_{\lambda D}^{D} \cdot C_D}{\varepsilon_{\lambda D}^{A} \cdot C_A} \cdot E_{approach\,1} \text{ where } F_{AD} = I_2 - I_1 S_1 \quad \text{and} \quad F_A = I_A S_2 \approx I_3 S_2$$

The FRET efficiency *E* can then be expressed as follows:

$$E_{approach\,1} = \frac{R_F - 1}{\frac{\varepsilon_{\lambda D}^{D} \cdot C_D}{\varepsilon_{\lambda D}^{A} \cdot C_A}}$$

However, the problem remains as to the data for C_D and C_A (unknown), and hence we move, instead, to *approach 2*, in which it is possible to directly test a range of data values to estimate the "cost" *J*, as follows:

$$E_{approach\,2} = \frac{I_D E\alpha}{I_D(1-E)\alpha + I_D E\alpha} \text{ where } I_D(1-E) \text{ and } I_D E\alpha \text{ is the unmixed fluorecent emissions (intensity).}$$

Here, we define a cost function *J* to represent the difference of FRET efficiency, using $E_{approach\,1}$ and $E_{approach\,2}$, as shown here:

$$J = \frac{\sum_1^n \left| E_{approach\,1} - E_{approach\,2} \right|}{n} = \frac{\sum_1^n \left| \frac{R_F - 1}{\frac{\varepsilon_{\lambda D}^{D} \cdot C_D}{\varepsilon_{\lambda D}^{A} \cdot C_A}} - \frac{I_D E\alpha}{I_D(1-E)\alpha + I_D E\alpha} \right|}{n}$$

The two unknows are then the *a* and the FRET-donor C_D and FRET-acceptor C_A concentration ratio (C_D/C_A). Therefore, *a* can be scanned with a range from 0 to 100, and the C_D/C_A with a range from 0.001 to 100 (with a stepwise size of 1), simultaneously. This is then narrowed to scan *a* with a range from 0.01 to 4 (stepwise size of 0.01) and C_D/C_A with a range from 0.01 to 2 (stepwise size of 0.005) for the two unknows. When the cost function *J* reaches a minimum, the two unknows of *a* and FRET-donor FRET-acceptor concentration ratio C_D/C_A can be estimated (see **Supplementary Figure 3**).

Supplementary Table: Fluorophore parameters for FRET distance calculations.

Parameters[1, 2]	CFP→YFP FRET1	YFP→RFP FRET2	CFP→RFP FRET3
Q_D	0.4	0.67	0.4
Q_A	0.67	0.25	0.25
ε_A (M^{-1} cm^{-1})	67000	50000	50000
$J(\lambda)$ (M^{-1} cm^{-1} nm^4)	1.53×10^{15}	2.27×10^{15}	1.45×10^{15}
R_0 (Å)	47.51	55.27	47.06

[1] Parameters were obtained from online fluorescent protein database FPbase (www.FPbase.org) and as originally from (1).

[2] Distance parameters were defined using data of TNFR1-FPs, calculated from data shown in **Supplementary Figure 4**, as follows, and as defined from original literature (2,3):

F_D = peak-normalised fluorescence spectrum of FRET donor,
Q_D = FRET donor quantum yield,
ε_A = extinction coefficient of the acceptor (M^{-1} cm^{-1}),
n = refractive index of the medium (an estimation of 1.33 is used for the table calculations),
κ^2 = orientation factor (an estimation of 2/3 ≈ 0.667 is used for the table calculations),
E = FRET efficiency,
R = is the distance between FRET donor and FRET acceptor.
Therefore J (λ) = FRET donor and FRET acceptor spectrum overlap integral and R_o = Förster Radius, distance (Å) between FRET donor and FRET acceptor, at which 50% FRET efficiency occurs is determined as shown:

$$J(\lambda) = \frac{\int_0^\infty F_D(\lambda)\varepsilon_A(\lambda)\lambda^4 d\lambda}{\int_0^\infty F_D(\lambda)d\lambda}$$

$$R_0 = 0.211 \cdot \sqrt[6]{\kappa^2 n^{-4} Q_D J(\lambda)}$$

$$E = \frac{1}{1 + \left(\frac{R}{R_0}\right)^6}$$

Supplementary Literature Cited:

1. Lambert TJ. FPbase: a community-editable fluorescent protein database. *Nat Methods.* 2019; 16: 277-278.
2. Wu P, Brand L. Resonance energy transfer: methods and applications. *Anal Biochem.* 1994; 218: 1-13.
3. Selvin PR. Fluorescence resonance energy transfer. Methods Enzymol. 1995; 246. 300-334.

Supplementary Figure 1. Dot Plot Profiles of Single Colour Controls. A single transfection experiment was acquired on both an LSR-II (**A**) and a Fortessa X-20 flow cytometer (**B**). Initial FSC-A/SSC-A data gating on cells (R1), then FSC-A/FSC-H data gating on singlets (R2). Data shown are fluorescence profiles of HEK293 cells transfected with pcDNA3 (empty vector, negative control), or single-colour controls pcDNA3.TNFR1-CFP or pcDNA3.TNFR1-YFP or pcDNA3.TNFR1-RFP expressing plasmids. Data shown is representative of multiple independently replicated experiments since single colour transfection controls are included in every FRET experiment.

Supplementary Figure 2. Correlation analysis for estimating spill-over effects. The bleed-through of each single (background-corrected) donor and acceptor fluorescence was determined using a series of linear regression analyses to determine the coefficient (slope relationship) between each possible pair of detection channels. Data are shown for both TNFR1 constructs and CD27 constructs obtained on either the LSRII or Fortessa-X20.

Supplementary Figure 3: Estimates of C_D/C_A as a function of cost *J*. The two unknows are the α and FRET-donor FRET-acceptor concentration ratio as C_D/C_A. These can be estimated by considering possible data outcomes. Hence, *first* a scan of possible α with a range from 0 to 100, and the C_D/C_A with a range from 0.001 to 100 (stepwise size of 1) is performed. The scan is repeated with a narrower range for α from 0.01 to 4 (stepwise size of 0.01) and C_D/C_A from 0.01 to 2 (stepwise size of 0.005). When the cost function *J* reaches a minimum, the two unknows of α and C_D/C_A can be estimated, as shown in either of the three parameter or two parameter output graphs. Thus, the method provides experimental estimates of concentration ratio of TNFR1-FP and TNFR1-FP (as C_D/C_A) for each of the FRET pairs.

Supplementary Figure 4: Donor-Acceptor distance estimates. TNFR1-FP FRET donor and TNFR1-FP FRET acceptor pair distance, based on single cell FRET-efficiency analysis. Data were obtained on the LSRII or Fortessa-X20 cytometer.

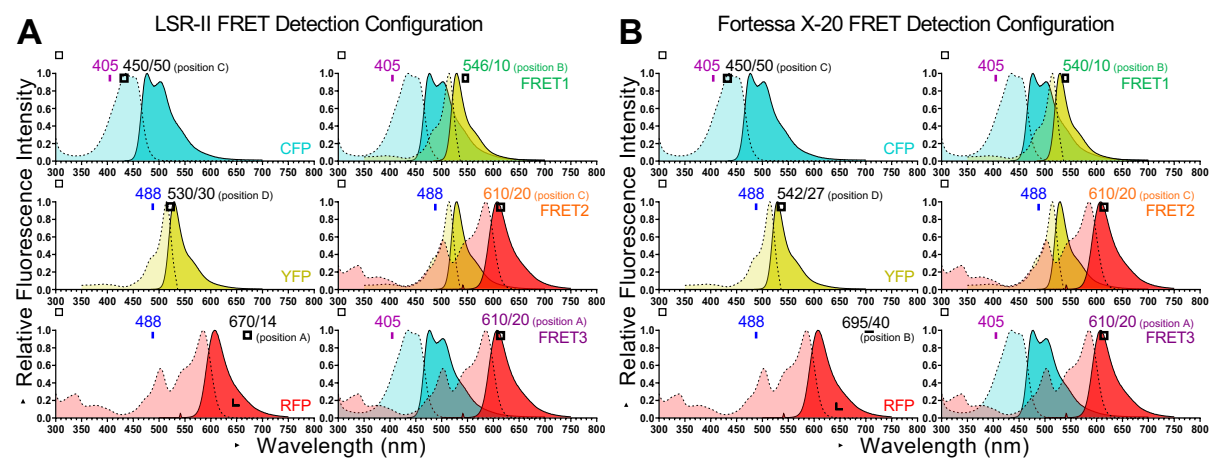
A
LSR-II FRET Detection Configuration
405
450/50 (position C)
CFP
405
546/10 (position B)
FRET1
488
530/30 (position D)
YFP
488
610/20 (position C)
FRET2
488
670/14
(position A)
RFP
405
610/20 (position A)
FRET3
Relative Fluorescence Intensity
Wavelength (nm)
B
Fortessa X-20 FRET Detection Configuration
405
450/50 (position C)
CFP
405
540/10 (position B)
FRET1
488
542/27 (position D)
YFP
488
610/20 (position C)
FRET2
488
695/40
(position B)
RFP
405
610/20 (position A)
FRET3
Relative Fluorescence Intensity
Wavelength (nm)

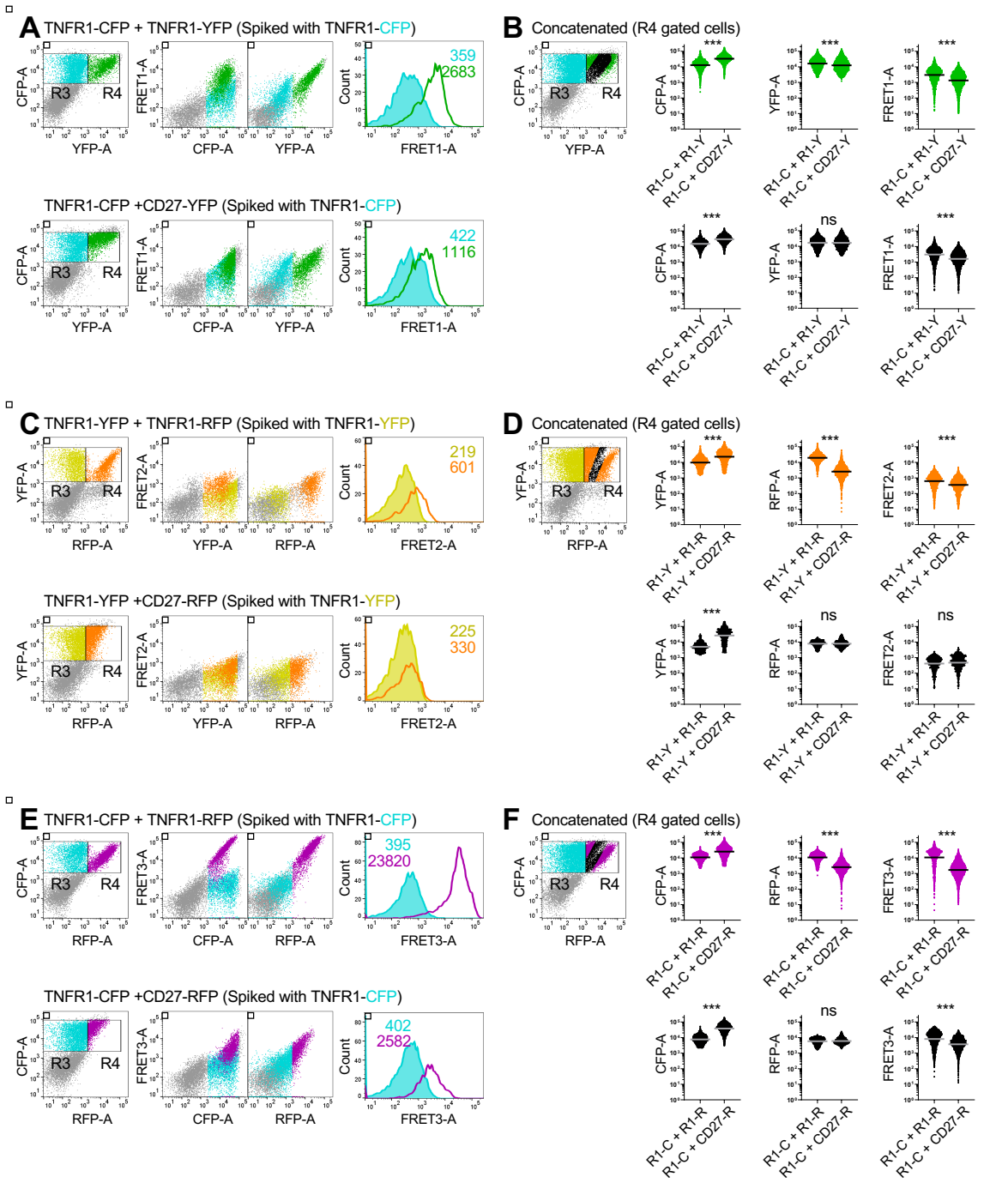
A
TNFR1-CFP + TNFR1-YFP (Spiked with TNFR1-CFP)
CFP-A
YFP-A
R3
R4
FRET1-A
CFP-A
YFP-A
Count
FRET1-A
359
2683
TNFR1-CFP +CD27-YFP (Spiked with TNFR1-CFP)
422
1116
B
Concatenated (R4 gated cells)
***
ns
R1-C + R1-Y
R1-C + CD27-Y
C
TNFR1-YFP + TNFR1-RFP (Spiked with TNFR1-YFP)
YFP-A
RFP-A
FRET2-A
219
601
TNFR1-YFP +CD27-RFP (Spiked with TNFR1-YFP)
225
330
D
R1-Y + R1-R
R1-Y + CD27-R
E
TNFR1-CFP + TNFR1-RFP (Spiked with TNFR1-CFP)
FRET3-A
395
23820
TNFR1-CFP +CD27-RFP (Spiked with TNFR1-CFP)
402
2582
F

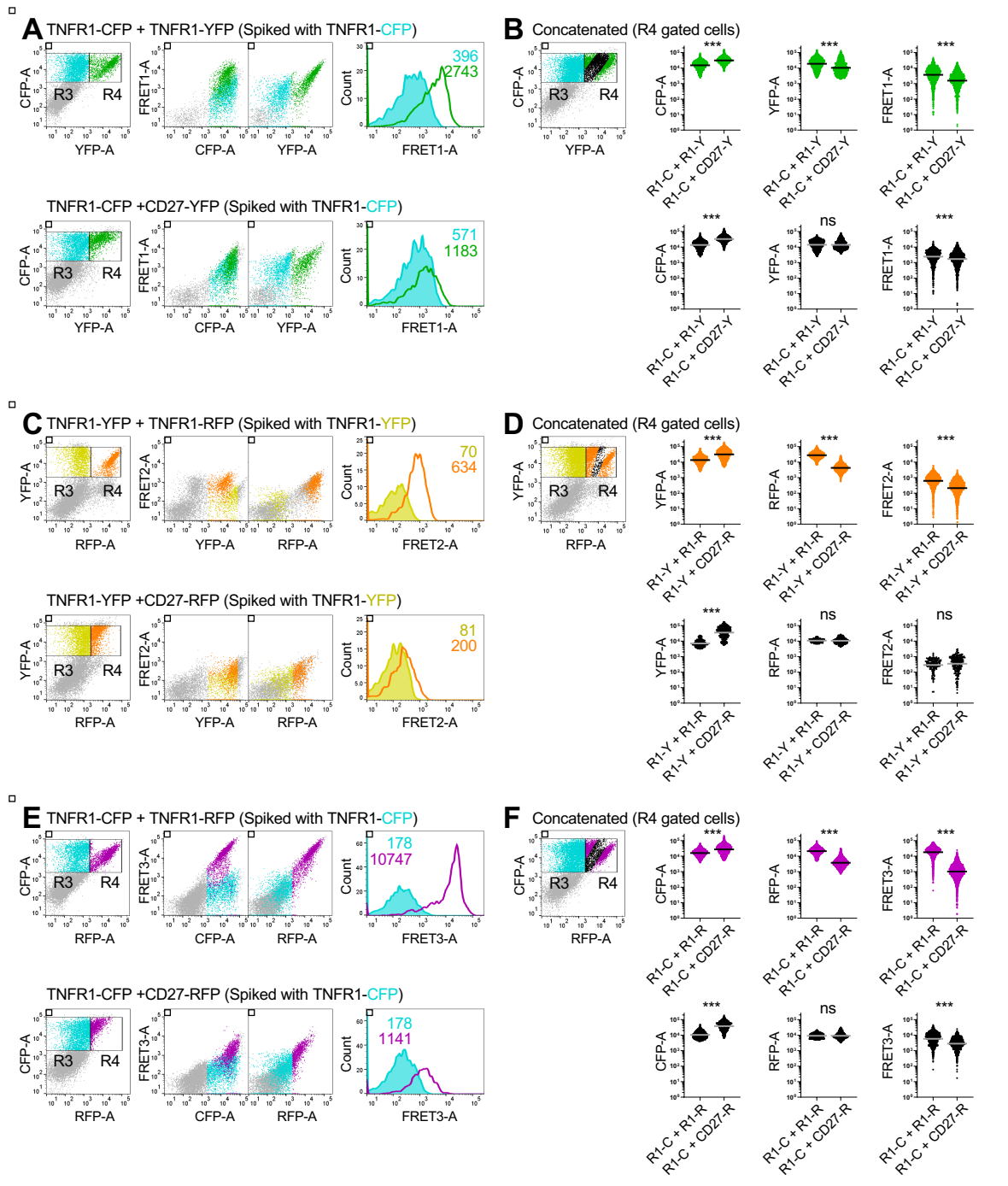
A
TNFR1-CFP + TNFR1-YFP (Spiked with TNFR1-CFP)
CFP-A
YFP-A
R3
R4
FRET1-A
CFP-A
YFP-A
Count
396
2743
FRET1-A
TNFR1-CFP +CD27-YFP (Spiked with TNFR1-CFP)
571
1183
B
Concatenated (R4 gated cells)
***
ns
R1-C + R1-Y
R1-C + CD27-Y
C
TNFR1-YFP + TNFR1-RFP (Spiked with TNFR1-YFP)
YFP-A
RFP-A
FRET2-A
70
634
TNFR1-YFP +CD27-RFP (Spiked with TNFR1-YFP)
81
200
D
R1-Y + R1-R
R1-Y + CD27-R
E
TNFR1-CFP + TNFR1-RFP (Spiked with TNFR1-CFP)
FRET3-A
178
10747
TNFR1-CFP +CD27-RFP (Spiked with TNFR1-CFP)
178
1141
F

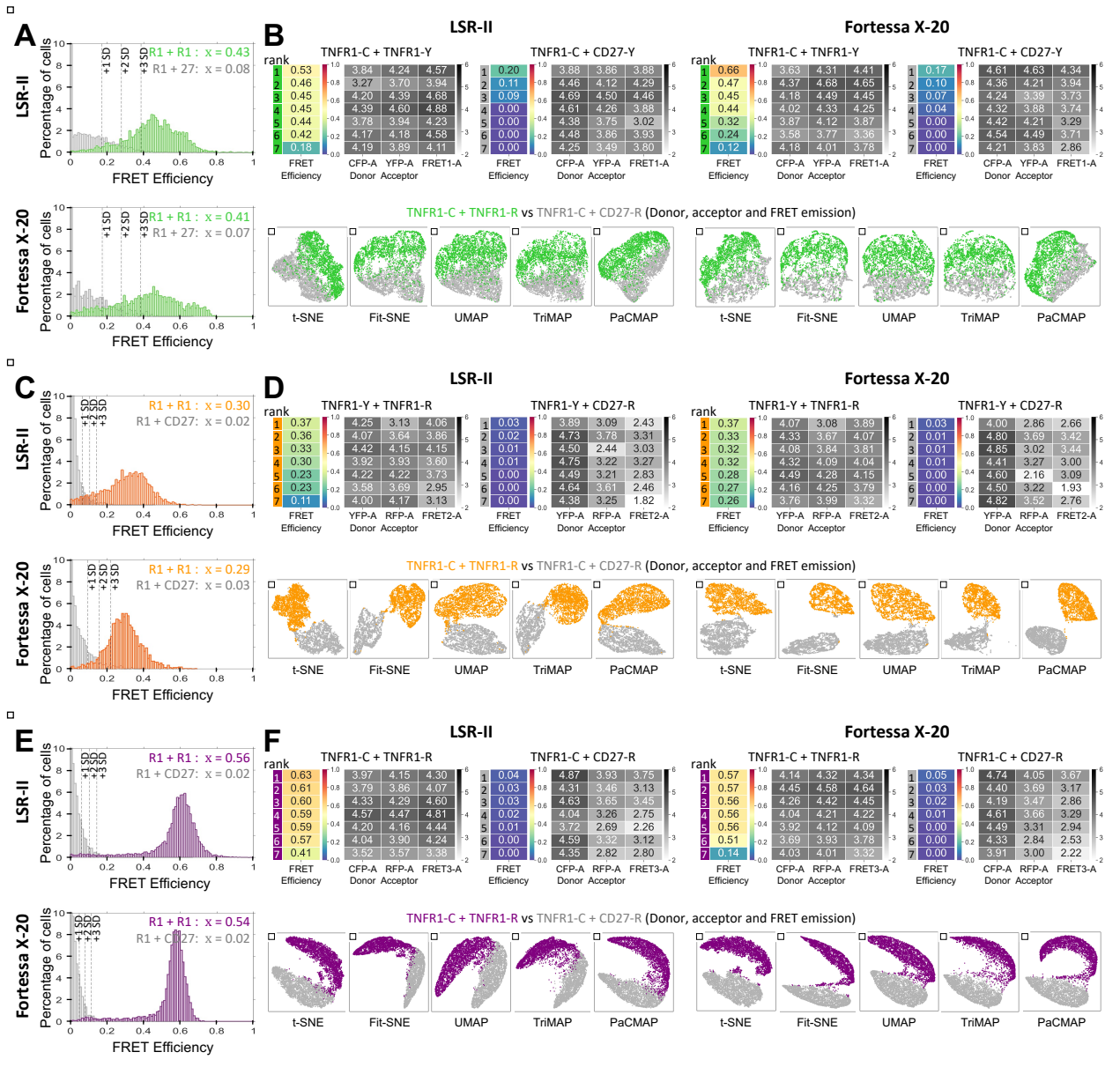
A
B
LSR-II
Fortessa X-20
Percentage of cells
FRET Efficiency
+1 SD
+2 SD
+3 SD
R1 + R1 : x = 0.43
R1 + 27: x = 0.08
R1 + R1 : x = 0.41
R1 + 27: x = 0.07
rank
TNFR1-C + TNFR1-Y
TNFR1-C + CD27-Y
CFP-A
YFP-A
FRET1-A
Donor
Acceptor
TNFR1-C + TNFR1-R vs TNFR1-C + CD27-R (Donor, acceptor and FRET emission)
t-SNE
Fit-SNE
UMAP
TriMAP
PaCMAP
C
D
R1 + R1 : x = 0.30
R1 + CD27: x = 0.02
R1 + R1 : x = 0.29
R1 + CD27: x = 0.03
TNFR1-Y + TNFR1-R
TNFR1-Y + CD27-R
YFP-A
RFP-A
FRET2-A
E
F
R1 + R1 : x = 0.56
R1 + CD27: x = 0.02
R1 + R1 : x = 0.54
R1 + CD27: x = 0.02
TNFR1-C + TNFR1-R
TNFR1-C + CD27-R
CFP-A
RFP-A
FRET3-A